Bulletin of the JSME Vol.8, No.1, 2021
Mechanical Engineering Journal

Modeling elastic lamina buckling in the unloaded aortic media

Atsutaka TAMURA*, Yuya KATO** and Koki MATSUMOTO**
*Department of Mechanical and Aerospace Engineering, Graduate School of Engineering, Tottori University
4-101 Koyama-minami, Tottori, Tottori 680-8552, Japan
E-mail: a-tamura@tottori-u.ac.jp
**Department of Mechanical Engineering, Graduate School of Sustainability Science, Tottori University
4-101 Koyama-minami, Tottori, Tottori 680-8552, Japan

Received: 27 May 2020; Revised: 16 September 2020; Accepted: 19 November 2020

Abstract
Mathematical modeling of the thoracic aorta is important for detecting extraordinary and unusual stress or strain distributions of the hypertensive aortic wall, even in early stages, and for understanding the development and progression of various cardiovascular diseases. In a freshly isolated aortic media, which mainly comprises elastic laminas (ELs) and smooth muscle layers (SMLs), circumferential EL waviness and longitudinal EL undulation are often observed because of the buckling of ELs, which is closely associated with residual stresses of ELs and SMLs in the aortic wall. However, the mechanism underlying EL buckling or specific mechanical interactions between EL and SML remains unclear. We hypothesized that the longitudinal EL undulation is likely formed by the superposition of the circumferential EL waviness along the aortic axis. Hence, a series of numerical simulations were conducted based on a design of experiments approach by implementing residual stresses. We identified that the prestress initially administered to ELs in the circumferential and axial directions, and the predefined internodal gap, which couples the EL and SML, are essential mechanical parameters to computationally reconstruct the circumferential EL waviness and the longitudinal EL undulation at an unloaded state. In addition, a mechanical balance between the assigned prestresses along the circumferential and axial directions is crucial for successful representation of structural buckling of EL in the unloaded aortic media. Although further study is required, we have verified that our hypothesis is reasonable in the current work. Moreover, the information we obtained here will greatly help improve understanding the roles of EL and SML in the aortic medial wall at the *in vitro* and *in vivo* states, while simultaneously providing a basis for more sophisticated computational modeling of the aorta.

Keywords: Elastic lamina (EL), Smooth muscle layer (SML), Waviness, Undulation, Buckling, Aortic media

1. Introduction

Cardiovascular diseases are a worldwide health concern, accounting for approximately 30% of total global mortality (WHO, 2018). In particular, hypertension is a common vascular disease that induces a mechanically abnormal loading environment on the aortic wall, leading to chronically disordered cardiovascular conditions with a loss of productive life years. In fact, hypertensive aorta is a primary risk factor for diverse concomitant diseases, including brain hemorrhage, myocardial infarction, and aortic aneurysm, and often results in arterial stiffening. Thus, changes in the mechanical properties of aortic tissues are considered to serve an essential role in the development of diseases and their progression over time. However, the mechanical events and the mechanisms underlying these clinical conditions have not to date been fully elucidated. Therefore, it is crucial to identify specific mechanical factors that trigger pathological and pathophysiological disorders associated with gradual progression or symptoms involving elevated blood pressure.

Developing a numerical model of *in vivo* simulation of cardiovascular tissues can address the patient-specific preclinical testing of a novel medical device (Castillo-Cruz et al., 2018; Caimi et al., 2020). To implement this approach, such models need to be based on an accurate estimation of the natural or intrinsic mechanical behavior of the

Paper No.20-00277
J-STAGE Advance Publication date : 26 November, 2020
[DOI: 10.1299/mej.20-00277]

aorta. Anatomically, the aortic wall is a composite structure composed of three layers: the inner layer or intima, the middle layer or media (a major component of the aorta), and the outer layer or adventitia. The media mainly consists of the elastic lamina (EL) and smooth muscle layer (SML), which controls the contraction and relaxation of the aorta and has a *Baumkuchen*-like structure with alternate layers of EL and SML in the physiological condition. When hypertension occurs, an aortic wall is constantly and preferentially stretched more in its circumferential direction compared with that under normal physiological conditions because of an increase in the vascular internal pressure. Thus, it is fundamentally important to reveal the factors that dominate the mechanical behavior or structural deformation of the aortic media, which can be closely associated with inhomogeneous stress and strain distributions from micro- to macrostructural viewpoints. In this sense, a finite element (FE) model is a useful and powerful research tool to investigate specific mechanical interactions between each component of the media, i.e., EL, SML, and stress fibers (SFs).

Recently, Iijima et al. (2012) found that EL in the unloaded aortic tissue shows waviness in the axial or longitudinal direction of the aortic media, which is termed as the waviness of EL ridge, as well as in the circumferential direction due to structural buckling. We hypothesized that this axial waviness of EL ridge, or longitudinal EL undulation, is a superposition of a series of circumferential EL waviness or buckled ELs along the aortic axis. Thus, we expect that a realistic FE model representing such a natural mechanical behavior in the aortic tissue can accurately predict wall stress distribution in a normotensive aorta while providing a noninvasive tool to examine hypertensive aorta.

Hence, we built a simplified FE model of the repeating lamellar unit (LU) structure of the media1 wall and stacked the multiple units in series along the aortic axis as a first step toward the development of a realistic FE model of the aorta. Further, we identified mechanical factors or a specific boundary condition to computationally reconstruct the longitudinal EL undulation and the circumferential EL waviness in the unloaded aortic media.

2. Methods

2.1 Theoretical model

The histological examination of the aortic wall showed that the majority of ELs running along the circumferential direction were wavy in the excised specimens (Matsumoto et al., 2004b), suggesting that ELs are compressed and buckled in the unloaded aortic tissue. On the other hand, SMLs are slightly stretched *in vitro* as a response to the wavy nature of ELs. According to the theoretical model (Fig. 1) proposed by Matsumoto et al. (2004a), an aortic medial wall is subjected to circumferential stretch *in vivo* due to the vascular internal pressure. On the contrary, a mechanical force between EL and SML should be balanced at the *in vitro* no-load condition (unloaded state), implying that only EL should be compressed at the "virtually" initial state (i.e., undeformed reference configuration) and that EL and SML would mutually maintain compressive and tensile residual stresses at the unloaded state (i.e., *in vitro* deformed configuration.

In our preceding work (Tamura and Kato, 2018), we successfully realized EL buckling using a simplified FE model, which represents only the arc portion of the aortic medial wall. As shown in Fig. 2, when a set of compressive prestresses initially given to EL were released, ELs showed buckling and reached the unloaded state at which EL and SML were subjected to compression and tension, respectively. In this case, while SMLs acted as a mechanical restriction or an interfering buffer to the overall marginal stretch along the circumferential direction, resulting in the EL buckling, EL behaved like a linear spring; thus, a set of ELs had a tendency to elongate in response to the initial compression.

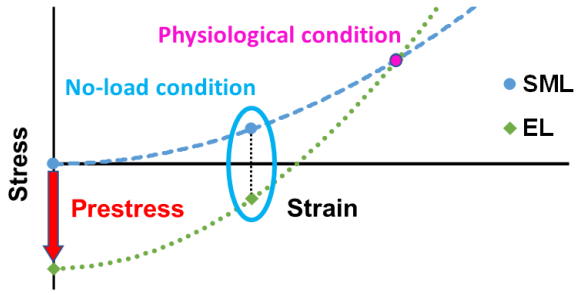

Fig. 1 Theoretical model of the aortic media. The unloaded medial tissue reaches an equilibrium state at the no-load condition. EL and SML are subjected to compression and tension, respectively, at the unloaded state (EL: elastic lamina, SML: smooth muscle layer). This concept was originally proposed by Matsumoto et al. (2004a and 2004b).

[DOI: 10.1299/mej.20-00277]

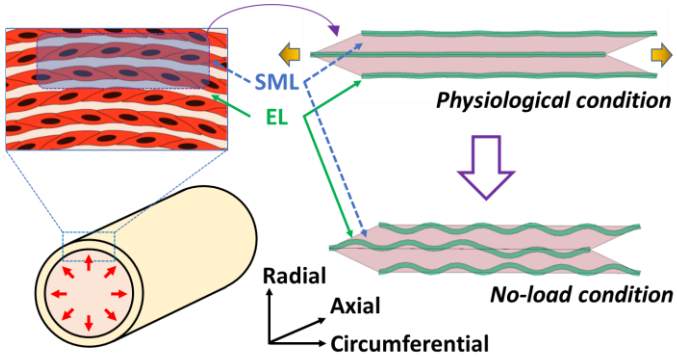

Fig. 2 Configuration change of the unit structure of the aortic media, depending on the vascular internal pressure. The ELs are taut and wavy at the physiological and no-load conditions, respectively (EL: elastic lamina, SML: smooth muscle layer).

2.2 Numerical model

The basic organization of the aortic media is known as a lamellar unit, i.e., LU, mainly consisting of EL and SML. In each LU, the EL is characterized by a lamellar sheet composed of thick, largely circumferential fibers and a set of interlamellar connecting fibers that construct a 3D cage-like structure around the SML (O'Connell et al., 2008). Figure 3 (bottom) shows the unit structure of the aortic media employed in this work. In reference to our preceding work (Tamura and Kato, 2018), we created the unit FE model using HyperMesh 2017 (Altair Engineering, Inc., Troy, MI, USA), in which two SMLs were sandwiched between three ELs. Each layer of ELs and SMLs contained 40 shell and 20 solid elements, respectively, and EL and SML were partially connected along the X-axis by shared nodes at an even interval, Dis X, i.e., 10, 20, 40, or 50 μm. In the present study, ELs were modeled assuming a linear elastic material with Young's modulus of 600 kPa (Fung, 1993), and the mechanical behavior of the passive contribution from SMLs is described by the Mooney-Rivlin strain energy density function, Ψ, as:

$$\Psi = A\,(I_1 - 3) + B\,(I_2 - 3) \tag{1}$$

where A = 17.23 (kPa) and B = 0.27 (kPa), which corresponded to Young's modulus of 100 kPa (Nagayama and Matsumoto, 2004) representing the stiffness of the isotropic ground matrix, while I_1 and I_2 are the first and second invariants of the right Cauchy–Green strain tensor, respectively. The local stress-strain behavior was calculated using the derivatives of Eq. (1). Basic material properties assigned for EL and SML are summarized in Table 1. These mechanical data were determined by referring to previously published literature (O'Connell et al., 2008; Matsumoto et al, 2004b; Lillie et al., 2012). Furthermore, SF was modeled using a one-dimensional bar element with an original diameter of 0.3 μm and Young's modulus of 1 MPa (Deguchi et al., 2006), obliquely connecting the upper, middle, and lower layers of EL. Since the available number of nodes was limited in this unit structure, the number of SFs in each layer was apparently increased by centuplicating the cross-sectional area of SF from 0.07 to 7.0 μm^2, while maintaining the number of SFs constant (82 elements). Consequently, a total volume of SFs occupied ~21% of the unit structure, and the number of elements contained in this unit structure amounted to 324.

Notably, since we aimed at realizing the longitudinal EL undulation (W_r) as well as the circumferential EL waviness (W) at the unloaded state, 10-unit structures were stacked and partially connected in series along the Y-axis at an even interval, Dis Y, i.e., 14, 28, 70, or 140 μm, as shown in Fig. 3 (top). In the current work, we assumed that W_r would strongly depend on DisY. Specifically, when the unit structures are tightly connected along the aortic axis with the smallest internodal gap, Dis Y = 14 μm, the anticipated waviness of EL ridge looks like a reverse C-shaped curve.

Table 1 Material properties assigned for the components contained in a unit structure of the aortic media.

	Young's modulus (kPa)	Poisson's ratio	Length (μm)	Height (μm)	Thickness (μm)
EL	600	0.450	200	3	14
SML	100	0.499	200	20	14

Length, height, and thickness represent the dimensions of the unit structure in the circumferential, radial, and longitudinal directions, respectively (EL: elastic lamina, SML: smooth muscle layer).

[DOI: 10.1299/mej.20-00277]

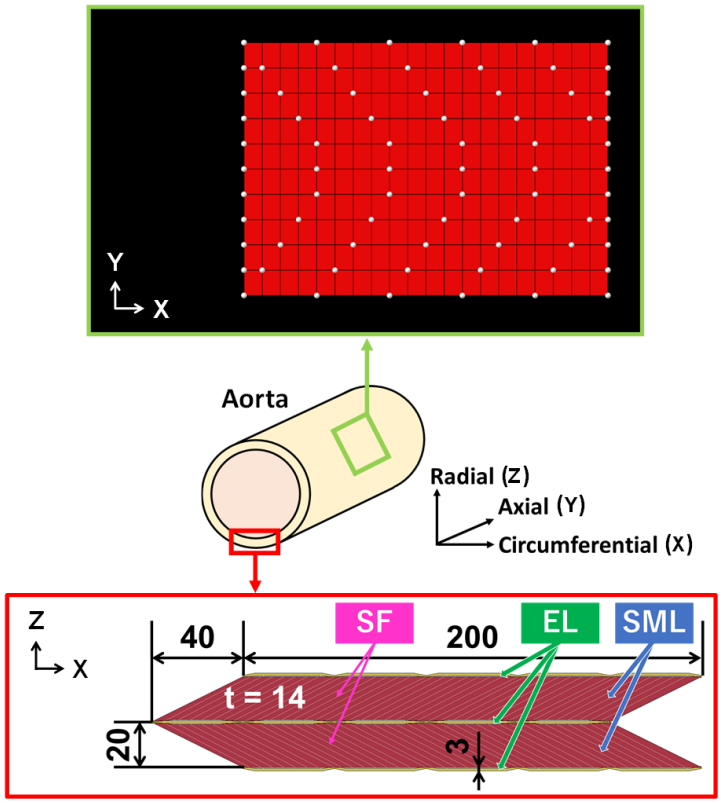

Fig. 3 Schematic of the unit structure of the aortic media (bottom) and an axially integrated model of unit structures (top). The shared nodes are highlighted for Dis X = 40 and Dis Y = 14 (Unit: μm). The X-, Y-, and Z-axes indicate the circumferential, longitudinal, and radial directions, respectively. Note that *t* denotes the thickness of the unit structure (EL: elastic lamina, SML: smooth muscle layer, SF: stress fiber).

2.3 Design of experiments

We employed the design of experiments (DOE) approach developed by Taguchi (1987) and utilized a special set of arrays. By properly selecting a specific number of independent factors or design variables and levels, the number of experiments to be conducted can be efficiently reduced. The integration of Taguchi's DOE and FE analysis has been used as a useful design tool in engineering fields (Tamura et al., 2001). Thus, we selected a pair of compressive prestresses, Pre-X and Pre-Y, which were applied to each integration point of EL along the X- and Y-axes (i.e., −120, −90, −60, or −30 kPa), and the internodal gaps, Dis X and Dis Y, along the circumferential and longitudinal directions as design variables.

A series of DOE numerical simulations with four levels and four design variables were then carried out based on a Graeco-Latin square method (Miyakawa, 2000). Specifically, a baseline DOE design consisting of Pre-X, Pre-Y, and Dis Y (n = 16) was combined with an additional four-level design variable, Dis X, and a total of 64 simulations were performed. As summarized in Table 2, "Case No." was determined as the combination of Case ID, 1–16, and the assigned value of Dis X, i.e., 10, 20, 40, and 50 μm. For instance, Case 1_40 represents the axially integrated FE model with Pre-X = −120 kPa, Pre-Y = −120 kPa, Dis X = 40 μm, and Dis Y = 70 μm. Similarly, Case 16_50 represents the integrated model with Pre-X = −30 kPa, Pre-Y = −30 kPa, Dis X = 50 μm, and Dis Y = 70 μm. All of the simulations were conducted using LS-DYNA v971 R10.0.0 (Livermore Software Technology Corp., Livermore, CA, USA).

[DOI: 10.1299/mej.20-00277]

Table 2 Allocation of selected design variables based on a Graeco-Latin square method (n = 16 × 4).

Case ID	Pre-X (kPa)	Pre-Y (kPa)	Dis X (μm)	Dis Y (μm)
1	−120	−120	*	70
2	−120	−90	*	28
3	−120	−60	*	14
4	−120	−30	*	140
5	−90	−120	*	28
6	−90	−90	*	70
7	−90	−60	*	140
8	−90	−30	*	14
9	−60	−120	*	140
10	−60	−90	*	14
11	−60	−60	*	70
12	−60	−30	*	28
13	−30	−120	*	14
14	−30	−90	*	140
15	−30	−60	*	28
16	−30	−30	*	70

Pre-X and Pre-Y are prestresses assigned for ELs in the initial undeformed configuration. Dis X and Dis Y are internodal gaps of shared nodes between EL and SML. Case ID defines a combination of Pre-X, Pre-Y, and Dis Y. *Note that Dis X can be replaced by 10, 20, 40, or 50 μm (EL: elastic lamina, SML: smooth muscle layer).

2.4 Analysis

As shown in Eq. (2) and Fig. 4a, a circumferential EL waviness, W, is defined as the ratio of a resultant elongated EL length, L_{EL}, and an end-to-end length of a deformed unit structure, L, in X-direction at the unloaded state. Similarly, as given by Eq. (3), a longitudinal EL undulation, W_r, is defined as the ratio of the resultant EL length along the ridge, L_{EL}', and the end-to-end length of a deformed integrated model, L_r, in Y-direction at the unloaded state (Fig. 4b). In the present study, W and W_r were computed from ELs in the middle layer of the unit structures axially connected in series and were averaged, avoiding its site-related variability. As it is discussed later, to identify predominantly influential factors contributing to the initiation of EL buckling at the no-load condition, we further conducted an analysis of variance on W for the entire cases (n = 64) and W_r for specific cases (n = 19) selected from the completed DOE simulations (n = 64). More specifically, we computed F-values for each selected design variable. By comparing the computed F-values and those listed in the F-distribution table, we successfully identified the effective design variables.

$$W = L_{EL} / L \tag{2}$$

$$W_r = L_{EL}' / L_r \tag{3}$$

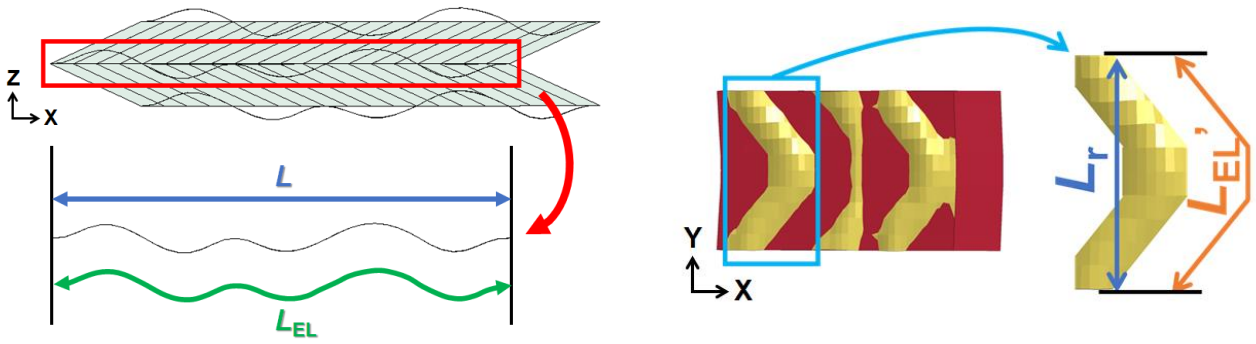

(a) Definition of L_{EL} and L of the unit structure. (b) Definition of L_{EL}' and L_r of the integrated model.

Fig. 4 Schematic of the resultant EL lengths (L_{EL} and L_{EL}') and end-to-end lengths of the unit structure and the integrated model (L and L_r) at the unloaded state. W and W_r are computed along the X- and Y-axes, respectively.

[DOI: 10.1299/mej.20-00277]

3. Results

3.1 Circumferential EL waviness

As shown in Fig. 5, the circumferential EL waviness, W, significantly decreased with the magnitude of compressive prestress, |Pre-X|, initially given ($P < 0.001$). Namely, a larger compressive prestress was preferred to realize EL buckling at the unloaded state because EL was likely to elongate almost linearly in response to the amount of initial compression when a set of prestresses were released; Eq. (2) suggests that W was sensitive to the change in L_{EL} because L was almost constant irrespective of the changes in Pre-X and Pre-Y. Thus, the resultant EL length at the unloaded state L_{EL} led to a larger value for −120 kPa cases in comparison with −30 kPa cases, which resulted in a larger value of W. Further, W gradually increased with the changes in Dis X and Dis Y, indicating that loose internodal gaps in both the circumferential and longitudinal directions are preferable to realize EL buckling at the unloaded state ($P < 0.001$). As we aimed to identify the specific mechanical parameters to computationally reconstruct both the circumferential EL waviness and the waviness of EL ridge, we excluded the cases in which the longitudinal EL undulation was not clearly observed ($n = 45$), and a further investigation was conducted for the remaining cases ($n = 19$) with $W = 1.082 \pm 0.038$ (mean ± SD) on average. Notably, most of the selected circumferential EL waviness ($n = 19$) fell within the range of reasonable values, 1.05–1.15, which was experimentally observed *in vitro* for the medial strips from the porcine aortas (Uno et al., 2010). Figure 6 demonstrates the normal X-stress distribution in the unit structure obtained at the initial and unloaded states. Obviously, ELs were subjected to compression at the initial state (i.e., undeformed reference configuration) along the circumferential (X) direction, while SMLs were subjected to tension at the unloaded state (i.e., deformed configuration) and maintained mechanical balance between EL and SML, as suggested by the theoretical model (Fig. 1).

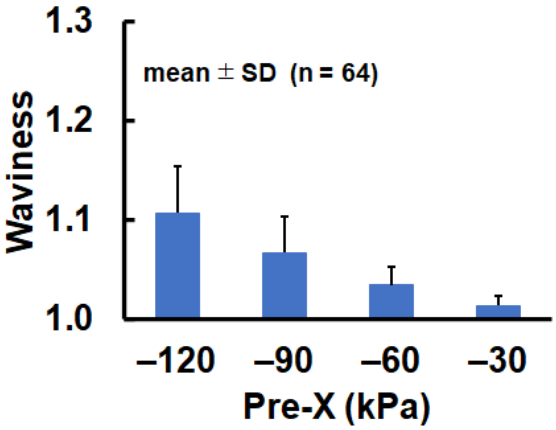

(a) Change in W with the circumferential prestress.

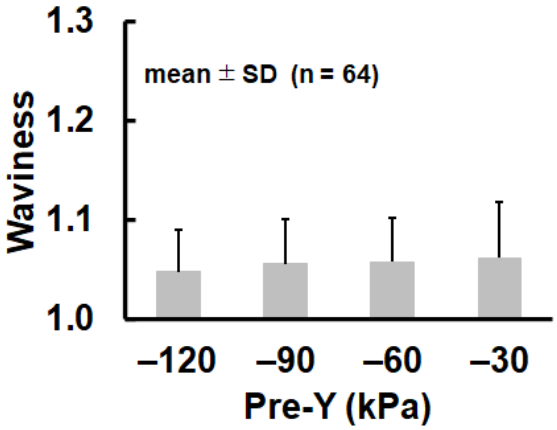

(b) Change in W with the longitudinal prestress.

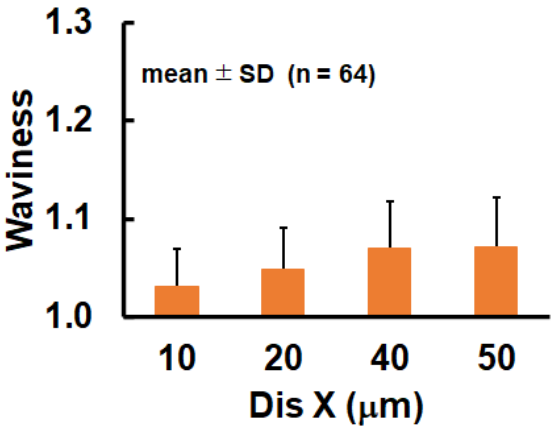

(c) Change in W with the circumferential internodal gap.

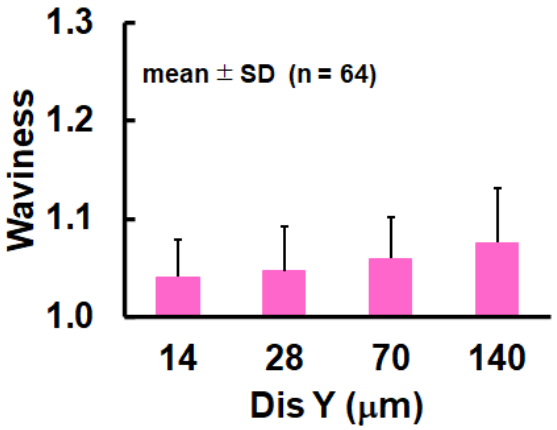

(d) Change in W with the longitudinal internodal gap.

Fig. 5 Changes in the circumferential EL waviness, W (mean ± SD), represented as a function of selected design variables ($n = 64$). Pre-X, Dis X, and Dis Y significantly influence the reproducibility of W at the unloaded state ($P < 0.001$).

[DOI: 10.1299/mej.20-00277]

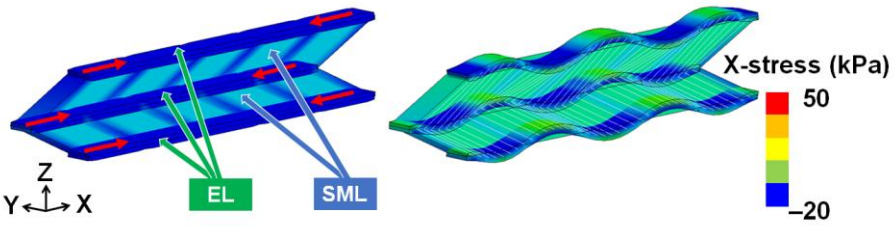

Fig. 6 Typical example of a contour plot (normal X-stress distribution) in the unit structure of an aortic media obtained at the initial (left) and unloaded (right) states. The red arrows indicate a set of compressive prestresses initially given to ELs.

3.2 Longitudinal EL undulation

We hypothesized that the longitudinal EL undulation is the superposition of a series of circumferential EL waviness along the aortic axis. In that sense, the reconstruction of circumferential EL waviness is primarily required to realize the longitudinal EL undulation at the unloaded state; that is, the magnitude of prestress given in X-axis should be larger than that in Y-axis, |Pre-X| > |Pre-Y| so that EL waviness preferentially occurs in the circumferential (X) direction rather than the longitudinal (Y) direction. In addition, as was found in our preceding work (Tamura and Kato, 2018), we confirmed that a weak prestress, Pre-X = −30 kPa, was insufficient, while a tight internodal gap, Dis X = 10 μm, was an overwhelming constraint to computationally represent EL waviness in the circumferential direction at the unloaded state (Fig. 5). Thus, the cases with $W < 1.010$ or $W_r < 1.010$ were excluded from further analysis, which amounted to $n = 45$. Based on these criteria, 19 cases with the distinct waviness of EL ridge were selected (Table 3) to identify the contributing factors to computationally realize the longitudinal EL undulation, W_r, as well as the circumferential EL waviness, W, at the unloaded state. As shown in Fig. 7, however, any specific trend was not seemingly found with respect to the pair of compressive prestresses, Pre-X and Pre-Y, and the internodal gaps, Dis X and Dis Y, although each of them would be indispensable for representing EL buckling at the unloaded state, while the average value of the longitudinal EL undulation, W_r, ranged from 1.1 to 1.3, i.e., $W_r = 1.212 \pm 0.089$ (mean ± SD). Figure 8 shows EL buckling patterns obtained at the unloaded state, highlighting that the longitudinal EL undulation is the superposition of a series of circumferential EL waviness along the aortic (Y) axis. Interestingly, even when the assigned internodal gaps along X-axis were relatively similar, i.e., Dis X = 40 or 50 (μm), the resultant values of W and W_r were completely different, depending on the other mechanical design variables, Pre-X, Pre-Y, and Dis Y.

Table 3 Summary of selected cases with both the circumferential EL waviness and the waviness of EL ridge ($n = 19$).

Case No.	***Pre-X (kPa)	Pre-Y (kPa)	***Dis X (μm)	***,‡Dis Y (μm)	W	W_r
1_40	−120	−120	40	70	1.136	1.208
1_50	−120	−120	50	70	1.149	1.291
2_40	−120	−90	40	28	1.114	1.059
3_20	−120	−60	20	14	1.077	1.170
3_40	−120	−60	40	14	1.103	1.224
3_50	−120	−60	50	14	1.116	1.216
5_40	−90	−120	40	28	1.086	1.303
6_40	−90	−90	40	70	1.096	1.082
6_50	−90	−90	50	70	1.109	1.167
7_20	−90	−60	20	140	1.090	1.046
7_40	−90	−60	40	140	1.116	1.020
8_20	−90	−30	20	14	1.037	1.206
8_50	−90	−30	50	14	1.077	1.216
10_20	−60	−90	20	14	1.014	1.172
11_40	−60	−60	40	70	1.056	1.034
11_50	−60	−60	50	70	1.069	1.118
12_40	−60	−30	40	28	1.034	1.200
12_50	−60	−30	50	28	1.047	1.198
16_50	−30	−30	50	70	1.029	1.013

***$P < 0.0001$ vs. W; ‡$P < 0.01$ vs. W_r

[DOI: 10.1299/mej.20-00277]

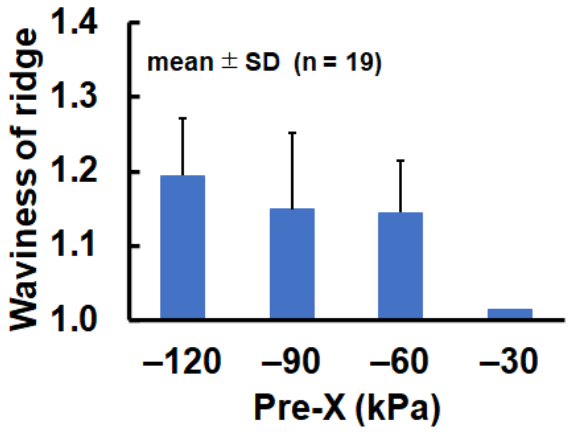

(a) Change in W_r with the circumferential prestress.

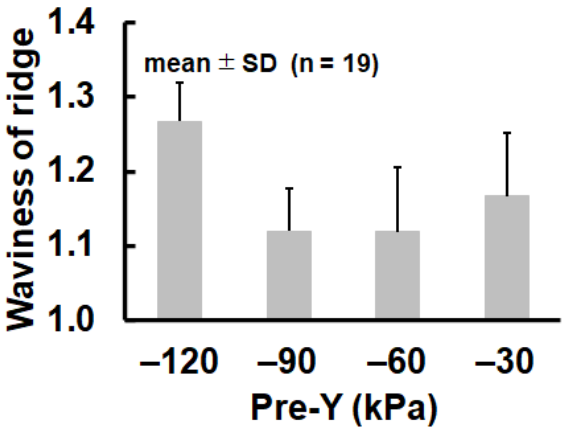

(b) Change in W_r with the longitudinal prestress.

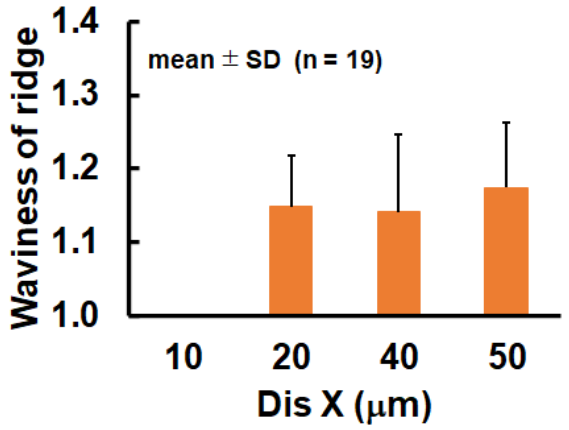

(c) Change in W_r with the circumferential internodal gap.

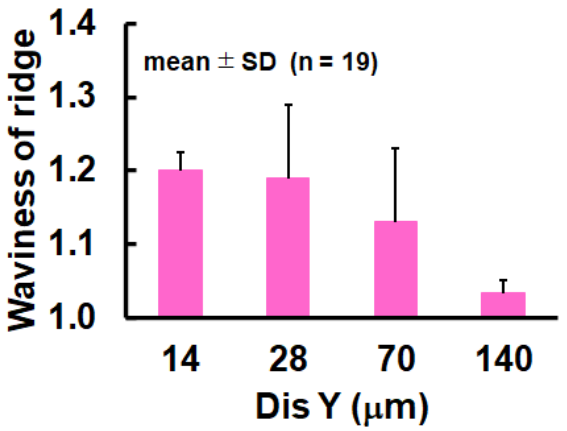

(d) Change in W_r with the longitudinal internodal gap.

Fig. 7 Changes in the longitudinal EL undulation or the waviness of EL ridge, W_r (mean ± SD), represented as a function of selected design variables (n = 19).

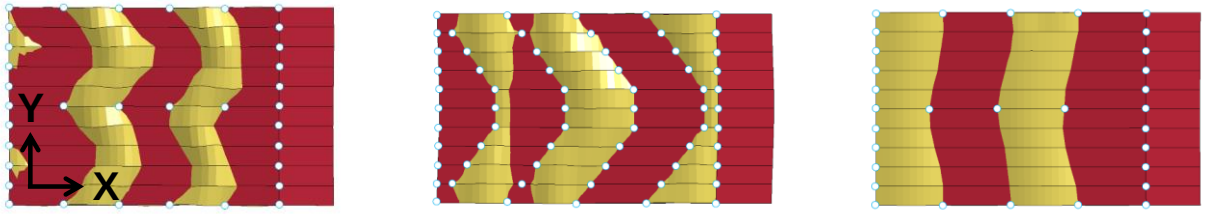

(a) Case 1_40 (b) Case 8_50 (c) Case 16_50

Fig. 8 Typical examples of the longitudinal EL undulation, W_r, obtained at the unloaded state. (Highlighted points are shared nodes between EL and SML.)

3.3 Additional analysis

Subsequently, a multiple regression analysis was conducted with the cases selected above (n = 19). Namely, W and W_r were set to be objective functions or dependent variables, while four design variables (Pre-X, Pre-Y, Dis X, and Dis Y) were regarded as independent variables as follows:

$$W = -0.00114\,\text{Pre-X} - 0.00019\,\text{Pre-Y} + 0.00038\,\text{Dis X} - 0.00133\,\text{Dis Y} + 0.89678 \tag{4}$$

$$W_r = -0.00062\,\text{Pre-X} - 0.00080\,\text{Pre-Y} + 0.00109\,\text{Dis X} - 0.00138\,\text{Dis Y} + 1.07273 \tag{5}$$

[DOI: 10.1299/mej.20-00277]

The coefficients of determination for the fitting curves were $R^2 = 0.999$ for W (Eq. (4)) and $R^2 = 0.536$ for W_r (Eq. (5)), respectively. Again, we confirmed that Pre-X, Dis X, and Dis Y were found to significantly contribute to reconstructing the circumferential EL waviness ($P < 0.0001$). Moreover, only the longitudinal internodal gap, Dis Y, was found to be a significant contributor to represent the longitudinal EL undulation ($P < 0.01$). The predicted values given by Eq. (4) closely matched with the values obtained by a set of numerical simulations ($n = 19$), while those given by Eq. (5) relatively matched well with the values obtained by the same set of numerical simulations. Nevertheless, since we employed a Graeco-Latin square method, the interaction between each parameter was not explicitly considered, and its effect might overshadow the specific contribution of each parameter to the computational reconstruction of the longitudinal EL undulation. Thus, an additional series of simulations ($n = 15$) were designed in which a boundary condition, |Pre-X| > |Pre-Y|, was maintained, and a fixed internodal gap condition was used, i.e., Dis X = 40 μm and Dis Y = 28 μm. In that case, EL buckling would readily occur along the circumferential direction, while the longitudinal EL undulation or the waviness of EL ridge would demonstrate both C and counter-C shapes (Fig. 9a). More specifically, Pre-X was set to −120, −90, and −60 kPa, and Pre-Y was scaled to 0%–100% of Pre-X, i.e., |Pre-Y| / |Pre-X| = 0, 0.25, 0.5, 0.75, and 1. In total, 15 simulations were performed, and W and W_r obtained at the unloaded state were analyzed. As we expected, when the applied prestresses were released, the circumferential EL waviness reached an almost constant value, $W = 1.12$, irrespective of the assigned Pre-Y (Fig. 9b). On the other hand, the longitudinal EL undulation varied with the change in the ratio of prestresses (Fig. 9c). Notably, W_r dramatically dropped down at the ratio of |Pre-Y| / |Pre-X| = 0.5, meaning that the waviness of EL ridge preferentially occurs when |Pre-X| and |Pre-Y| are almost equivalent in magnitude and |Pre-Y| is larger than 30 kPa, i.e., |Pre-X| > 60 kPa.

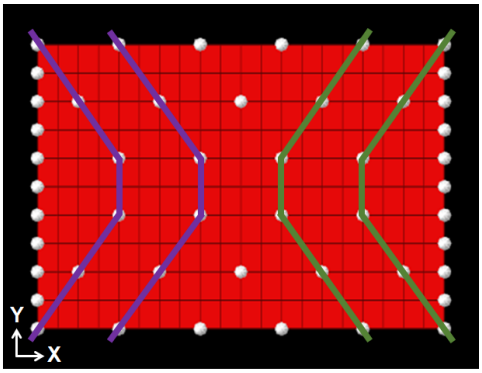

(a) Anticipated patterns of EL ridge with the internodal gap condition of Dis X = 40 and Dis Y = 28 (μm).

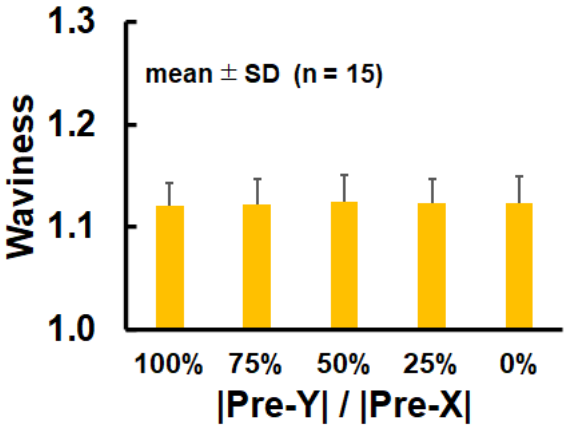

(b) Change in W with the ratio of |Pre-Y| / |Pre-X|.

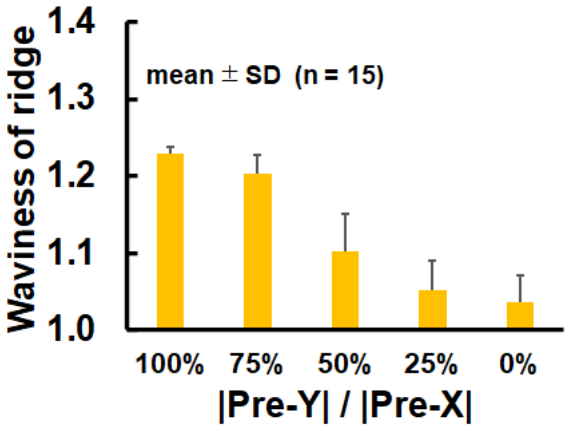

(c) Change in W_r with the ratio of |Pre-Y| / |Pre-X|.

Fig. 9 Changes in circumferential EL waviness, W, and waviness of EL ridge, W_r (mean ± SD), represented as a function of the ratio of a pair of assigned prestresses ($n = 15$).

[DOI: 10.1299/mej.20-00277]

4. Discussion

To computationally represent the natural mechanical behavior of EL, e.g., EL buckling at the unloaded state, considering residual stresses of EL and SML is indispensable. It was analytically revealed that even a small residual stress at the unloaded state significantly reduce the high stress concentration on the arterial inner wall at the loaded state, which is induced by vascular dilatation (Chuong and Fung, 1986); this is also the case even with the hypertensive aorta, implying that abnormal signs or symptoms relevant to pathophysiological disorder can be detected in stress and strain distributions in the aortic wall. Of note, it is known that arterial stiffening is a major determinant of hypertension and vice versa (Heusinkveld et al., 2018). Nevertheless, arterial stiffness measurement in a macroscopic point of view does not provide specific insight into the effect of residual stress heterogeneity nor strain inhomogeneity in the vascular micro- and macro-structures. Thus, development of a methodology for implementing residual stresses into aortic medial wall is an important step toward computational model-based predictions of the hypertensive aorta because we need to understand at first what kind of heterogeneity or inhomogeneity can be accepted as a normal and healthy condition of the medial wall. Therefore, the primary goal of this study was to identify mechanical design parameters to realize EL buckling in the unloaded aortic media.

As for the circumferential EL waviness obtained at the selected cases (n = 19), the average value, W = 1.082 ± 0.038 (mean ± SD), agreed with the measured values reported in a previous study (Uno et al., 2010), indicating that the range of initial prestresses assigned for EL in this study was comparably reasonable. Notably, the residual stresses of EL and SML obtained at the unloaded state were compressive and tensile, respectively, and quantitatively equivalent to the values estimated by the prior works, i.e., ±10 kPa (Breslavsky and Amabili, 2018; Liu et al., 2019; Matsumoto et al., 2004a and 2004b). As a preliminary study, we applied a set of tensile prestresses along the aortic axis to the initial reference configuration of an integrated FE model. However, we found that compressive prestress should be initially given in Y-direction, because EL is likely to shrink longitudinally when the tensile prestress axially given is released, preventing the EL buckling formed in the circumferential direction. Our computational model also showed that any resultant cross-sectional force, including EL and SML obtained at the unloaded state, was almost zero along its circumferential direction. Intrinsically, however, the aorta is structurally a long tube with curvature, and is constrained by the spine, ligaments, and the surrounding internal organs, which would affect the microstructural feature of the aortic tissue and the distribution of residual stress or strain. Thus, the contribution of other biological factors should be further investigated in our follow-up work. Another point to note is that, although the number of interlamellar SFs likely contributes to the increase in the stiffness of LU, its contribution was relatively minor to bear the bulk of load applied in the circumferential direction. Our preliminary study also revealed that the SF area would be an effective design variable as far as the assigned values fell within a reasonable range, in other words, up to a 100-fold increase in the SF area, which was equivalent to a condition wherein ~21% of the unit structure volume was occupied by SFs. Moreover, the slight tendency suggests that SFs would partly bear the tensile load at the unloaded state. Nonetheless, more than a 100-fold increase in the SF area would be practically ineffective (Tamura and Kato, 2018), and we adopted the devised SF area, 7.0 μm^2, in the current work.

As for the longitudinal EL undulation or the waviness of EL ridge, the numerical results obtained in the selected cases (n = 19), W_r = 1.212 ± 0.089 (mean ± SD), were relatively consistent with the corresponding experimental result (Iijima et al., 2012). Interestingly, W_r = ~1.2 is equivalent to an axial pre-stretch commonly applied to the computational models of the aorta (Heusinkveld et al., 2018; Gültekin et al., 2019), suggesting that W and W_r would completely vanish at the physiological condition with the increase in vascular internal pressure. When the magnitude of |Pre-Y| is larger than that of |Pre-X|, EL buckling would preferentially occur along the longitudinal direction rather than the circumferential direction, irrespective of the assigned internodal gaps. This indicates that a mechanical balance between Pre-X and Pre-Y is important for regulating the EL buckling behavior, while |Pre-X| = 30 (kPa) was too small to induce the circumferential EL waviness. In addition, a relatively loose connection between ELs and SMLs is preferred to realize EL buckling. For instance, Dis X = 10 (μm) prevented the circumferential EL buckling ($W \approx 1.0$) and resulted in W_r = ~1.0 in the longitudinal direction because an excessive mechanical constraint was imposed. In summary, we have found that the following boundary conditions are preferred to successfully realize the structural buckling of EL at the unloaded state along the circumferential and longitudinal directions:

1) |Pre-X| > |Pre-Y| where |Pre-Y| / |Pre-X| > 0.5
2) |Pre-X| > 60 kPa

[DOI: 10.1299/mej.20-00277]

3) |Dis X| > 10 μm

To the best of our knowledge, this is the first study involving the mechanical interaction between EL and SML in the aortic media. Even though our focus was primarily placed on the no-load condition (unloaded state) of the excised tissue *in vitro*, the specific boundary conditions identified here, a combination of Pre-X, Pre-Y, Dis X, and Dis Y will be useful and readily applicable to build a realistic FE model of aorta. However, a few limitations of the study should be noted. Firstly, collagen fibers were not included in the unit structure. It is known that EL dominates a mechanical response of the aortic media at low strains, 0%–20%, on the basis of a deformed configuration at the unloaded state, while collagen fibers likely contribute at high strains, 30%–50% (Clark et al., 2015; Thunes et al., 2016 and 2018). However, we paid close attention to the *in vitro* condition, and collagen fibers would not be a main load bearer in the current loading environment. Secondly, the integrated FE model is based on the passive constitutive and structural information obtained from the literature and mechanical testing. Thus, investigating the active contraction of SML should be considered in future work as its importance in cellular biomechanics has been reported (Nagayama et al., 2015; Nagayama, 2019). Thirdly, the effectiveness of the design variables may depend on the adopted modeling technique; for example, we allowed EL separation from SML and its penetration into SML to represent EL buckling, which may not be the case *in vivo*. In our preceding work (Tamura and Kato, 2018), we confirmed that the circumferential EL waviness and residual stresses in EL and SML computed at the *in vitro* unloaded state were comparable well with the measured and estimated values. However, available test data is still limited to fully support the validity of our modeling approach. In addition, we assumed that the SML is an isotropic material for simplicity whereas the aortic media is inherently anisotropic. Thus, further studies should be conducted spanning multiple (from micro- to macro-) scales so as to enhance a better understanding of the arterial mechanics and vascular biomechanics.

5. Conclusion

In conclusion, a series of numerical simulations were conducted using a simplified medial FE model. We identified specific mechanical conditions to represent the circumferential EL waviness as well as the longitudinal EL undulation or the waviness of EL ridge, and successfully realized the structural buckling of EL in the unloaded aortic media by implementing the residual stresses. Moreover, we revealed that the longitudinal EL undulation was a superposition of the circumferential EL waviness connected in series along the aortic axis. Although further study is required, our findings will help understand the roles of EL and SML in the aortic medial wall at the *in vitro* and *in vivo* states. We also expect that this modeling technique will be a useful tool in the future for interpreting stress distribution relevant to vascular physiology at normal and pathological states.

Acknowledgment

This study was supported in part by AMED-CREST (JP20gm0810005) and JSPS KAKENHI Grant Number JP19K12782.

References

Breslavsky, I. and Amabili, M., Nonlinear model of human descending thoracic aortic segments with residual stresses, Biomech Model Mechanobiol, Vol.17 (2018), pp.1839–1855.

Caimi, A., Pasquali, M., Sturla, F., Pluchinotta, F.R., Giugno, L., Carminati, M., Redaelli, A. and Votta, E., Prediction of post-stenting biomechanics in coarcted aortas: a pilot finite element study, J Biomech, Vol.105 (2020), 109796.

Castillo-Cruz, O., Pérez-Aranda, C., Gamboa, F., Cauich-Rodríguez, J.V., Mantovani, D. and Avilés, F., Prediction of circumferential compliance and burst strength of polymeric vascular grafts, J Mech Behav Biomed Mater, Vol.79 (2018), pp.332–340.

Chuong, C.J. and Fung, Y.C., On residual stresses in arteries, J Biomech Eng, Vol.108 (1986), pp.189–192.

Clark, T.E., Lillie, M.A., Vogl, A.W., Gosline, J.M. and Shadwick, R.E., Mechanical contribution of lamellar and interlamellar elastin along the mouse aorta, J Biomech, Vol.48 (2015), pp.3599–3605.

Deguchi, S., Ohashi, T. and Sato, M., Tensile properties of single stress fibers isolated from cultured vascular smooth mus-cle cells, J Biomech, Vol.39 (2006) pp.2603–2610.

[DOI: 10.1299/mej.20-00277]

Fung, Y.C., Biomechanics: Mechanical Properties of Living Tissues. 2nd ed. (1993), pp.250–251, Springer-Verlag, New York.

Gültekin, O., Hager, S.P., Dal, H. and Holzapfel G.A., Computational modeling of progressive damage and rupture in fibrous biological tissues: application to aortic dissection. Biomech Model Mechanobiol, Vol. 18 (2019), pp.1607–1628.

Heusinkveld, M.H.G., Quicken, S., Holtackers, R.J., Huberts, W., Reesink, K.D., Delhaas, T. and Spronck, B., Uncertainty quantification and sensitivity analysis of an arterial wall mechanics model for evaluation of vascular drug therapies, Biomech Model Mechanobiol, Vol.17 (2018), pp.55–69.

Iijima, S., Nagayama, K., Nakamura, S., Yokota, H. and Matsumoto, T., Observation of 3D micro-structure of rabbit thoracic aortic walls using three-dimensional internal structure microscope, Proceedings of the 23rd JSME Conference on Frontiers in Bioengineering (2012), Paper No. C117 (in Japanese).

Lillie, M.A., Armstrong, T.E., Gérard, S.G., Shadwick, R.E. and Gosline, J.M., Contribution of elastin and collagen to the inflation response of the pig thoracic aorta: assessing elastin's role in mechanical homeostasis, J Biomech, Vol.45 (2012), pp.2133–2141.

Liu, H., Zhang, M., Liu, M., Martin, C., Cai, Z. and Sun, W., Finite element simulation of three dimensional residual stress in the aortic wall using an anisotropic tissue growth model, J Mech Behav Biomed Mater, Vol.92 (2019), pp.188–196.

Matsumoto, T., Goto, T., Furukawa, T. and Sato, M., Residual stress and strain in the lamellar unit of the porcine aorta: experiment and analysis, J Biomech, Vol.37 (2004a), pp.807–815.

Matsumoto, T., Goto, T. and Sato, M., Microscopic residual stress caused by the mechanical heterogeneity in the lamellar unit of the porcine thoracic aortic wall, JSME Int J, Series A, Vol.47 (2004b), pp.341–348.

Miyakawa, M., Technology for getting quality what the Taguchi method has brought us (2000), JUSE Press, Ltd. (in Japanese).

Nagayama, K. and Matsumoto, T., Mechanical anisotropy of rat aortic smooth muscle cells decreases with their contraction (Possible effect of actin filament orientation), JSME Int J, Series C, Vol.47 (2004), pp.985–991.

Nagayama, K., Saito, S. and Matsumoto, T., Multiphasic stress relaxation response of freshly isolated and cultured vascular smooth muscle cells measured by quasi-in situ tensile test, Bio-Med Mater Eng, Vol.25 (2015), pp.299–312.

Nagayama, K., Biomechanical analysis of the mechanical environment of the cell nucleus in serum starvation-induced vascular smooth muscle cell differentiation, J Biomech Sci Eng, Vol.14 (2019), 19-00364.

O'Connell, M.K., Murthy, S., Phan, S., Xu, C., Buchanan, J., Spilker, R., Dalman, R.L., Zarins, C.K., Denk, W. and Taylor, C.A., The three-dimensional micro- and nanostructure of the aortic medial lamellar unit measured using 3D confocal and electron microscopy imaging, Matrix Biology, Vol.27 (2008), pp.171–181.

O'Rourke, M., Mechanical principles in arterial disease, Hypertension, Vol.26 (1995), pp.2–9.

Taguchi, G., The system of experimental design: engineering methods to optimize quality and minimize costs (1987), Quality Resources.

Tamura, A., Furusu, K., Kato, C., Miki, K., Hasegawa, J. and Yang, K.H., Tibial mid-shaft injury mechanism in frontal automotive crashes, Proceedings of the 17th International Technical Conference on the Enhanced Safety of Vehicles (2001), Paper No. 355.

Tamura, A. and Kato, Y., Reproduction of kinematic behavior of elastic lamellae in the thoracic aortic media, Proceedings of ASME 2018 International Mechanical Engineering Congress and Exposition (2018), Paper No. IMECE2018-87242.

Thunes, J.R., Pal, S., Fortunato, R.N., Phillippi, J.A., Gleason, T.G., Vorp, D.A. and Maiti, S., A structural finite element model for lamellar unit of aortic media indicates heterogeneous stress field after collagen recruitment, J Biomech, Vol.49 (2016), pp.1562–1569.

Thunes, J.R., Phillippi, J.A., Gleason, T.G., Vorp, D.A. and Maiti, S., Structural modeling reveals microstructure-strength relationship for human ascending thoracic aorta, J Biomech, Vol.71 (2018), pp.84–93.

Uno, Y., Nagayama, K. and Matsumoto, T., Observation of microscopic deformation in the porcine thoracic aortic wall during circumferential stretch, Proceedings of JSME Annual Meeting (2010), Paper No. T0201-3-6 (in Japanese).

World Health Organization, Global health estimates 2016: deaths by cause, age, sex, by country and by region, 2000-2016, Geneva, WHO (2018).

[DOI: 10.1299/mej.20-00277]